

# Three-Particle Correlations in Simple Liquids

K. Zahn, G. Maret, C. Ruß and H.H. von Grünberg

*Universität Konstanz, Fachbereich Physik, P.O.B. 5560, 78457 Konstanz, Germany*

(Dated: May 22, 2019)

We use video microscopy to follow the phase-space trajectory of a two-dimensional colloidal model liquid and calculate three-point correlation functions from the measured particle configurations. Approaching the fluid-solid transition by increasing the strength of the pair-interaction potential, one observes the gradual formation of a crystal-like local order due to triplet correlations, while being still deep inside the fluid phase. Furthermore, we show that in a strongly interacting system the Born-Green equation can be satisfied only with the full triplet correlation function but not with three-body distribution functions obtained from superposing pair-correlations (Kirkwood superposition approximation).

PACS numbers:

Our current understanding of the structure of simple fluids is based on the  $n$ -body distribution functions  $g^{(n)}$ , measuring the probability density of finding two, three, and more particles at specified positions in space. When the total potential energy of a liquid is given by a sum of pair-potentials, all of its thermodynamic properties can be calculated by means of the pair-correlation function  $g(r) \equiv g^{(2)}(r)$  and its density ( $\rho$ ) and temperature ( $T$ ) derivatives. However, the latter two quantities,  $\partial g(r)/\partial \rho$  and  $\partial g(r)/\partial T$ , explicitly depend on the triplet correlation function, even if the particle interactions are only pair-wise additive [1]. Explicit knowledge of triplet correlations is also required in perturbation theories for static fluid properties [2], in theories of transport properties [3], of solvent reorganization processes around solutes [4] and of systems under shear-flow [5]. Most of our knowledge on triplet correlations come from computer simulation studies of hard-sphere-fluids [6], Lennard-Jones (LJ) fluids [7, 8, 9, 10, 11, 12, 13], electrolyte systems [14, 15], and Yukawa fluids [16]. In the overwhelming majority, these papers are concerned with testing Kirkwood's superposition approximation (KSA) [17] for the triplet distribution function. By contrast, semi-analytical theories for  $g^{(3)}$  beyond the KSA are rather rare [13, 18, 19, 20, 21]. However, despite the long-standing theoretical interest in its properties, it has never been possible to measure three-particle correlations directly. One indirect way to obtain experimental information on  $g^{(3)}$  is based on the relationship between the isothermal pressure derivative of the fluid structure factor  $\partial S(q)/\partial P$  and the triplet distribution function [1], a relationship which has been systematically exploited by Egelstaff and co-workers in rare-gas systems [22].

The present Letter reports on the first direct measurement of  $g^{(3)}$ . We use video-microscopy to follow the phase-space trajectory of a two-dimensional colloidal model liquid with well-defined pair-interaction potentials and calculate three-point correlation functions from the measured particle configurations. We show that the three particle correlation function in the liquid phase reveal the

formation of a crystal-like local order near each particle, thus announcing the transition to an ordered phase, and that the Born-Green equation [23], one of the fundamental equations of statistical mechanics, can be satisfied only if triplet correlations are taken fully into account. The preparation of the samples and the experiments have been carried out as described in [24]: Paramagnetic colloids (diameter  $d = 4.5 \mu\text{m}$ ) are confined by gravity to a water/air interface whose flatness can be controlled within less than a micron. A magnetic field  $B$  applied perpendicular to the interface induces in each particle a magnetic moment  $M = \chi B$  which leads to a repulsive dipole-dipole pair-interaction energy of  $\beta u(r) = \Gamma/(\sqrt{\pi\rho}r)^3$  with the interaction strength given by  $\Gamma = \beta(\mu_0/4\pi)(\chi B)^2(\pi\rho)^{3/2}$  ( $\beta = 1/kT$  the inverse temperature,  $\chi$  the susceptibility).  $\Gamma$  is the only parameter determining the phase-behavior of the system: for  $\Gamma < 57$  the system is liquid, for  $\Gamma > 60$  it is solid, and in between, i.e. for  $57 < \Gamma < 60$ , it shows a hexatic phase [24, 25]. We here analyze three different  $\Gamma$  ( $\Gamma = 4, 14, 46$ ), where the system is deep in the liquid phase, and use for each (well equilibrated) system about 200 statistically independent configurations with approximately 500 particles, recorded using digital video-microscopy with subsequent image-processing on the computer. From the measured particle configurations,  $g^{(3)}$  is obtained by computing the average count per configuration of a particular kind of triplet, divided then by the appropriate normalizing factor.

Triplet correlations can be characterized by the ratio between the full triplet distribution function  $g^{(3)}$  and its approximated form based on the KSA  $g_{SA}^{(3)} = g(\mathbf{r}_1)g(\mathbf{r}_2)g(\mathbf{r}_3)$ . This ratio is given by what is called the triplet correlation function, denoted here by  $G(\mathbf{r}_1, \mathbf{r}_2, \mathbf{r}_3)$ . Thus,  $g^{(3)} = g_{SA}^{(3)}G$ . All pair correlations in  $g^{(3)}$  are included in  $g_{SA}^{(3)}$ , while the extent of the intrinsic correlations due to the simultaneous presence of a triplet of particles at positions  $\mathbf{r}_1, \mathbf{r}_2, \mathbf{r}_3$  is quantified through the function  $G$ , which thus defines the local structure of the fluid beyond that expressed by the pair-correlation

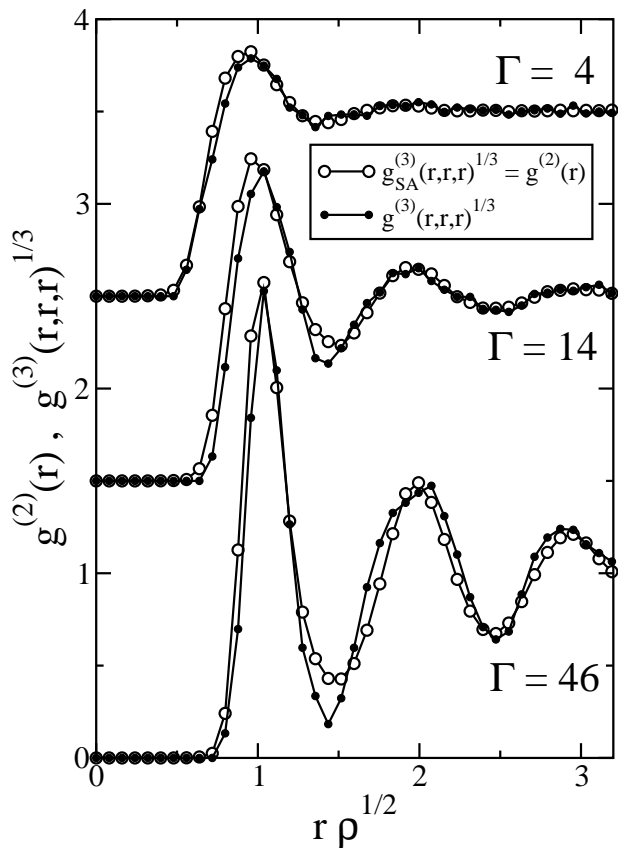


FIG. 1: Triplet distribution functions  $g^{(3)}$  as a function of the side length of an equilateral triangle, as computed from measured particle configurations for different  $\Gamma$ .  $g_{SA}^{(3)}$  is the triplet distribution function in the Kirkwood superposition approximation which on taking the cubic root,  $\sqrt[3]{g_{SA}^{(3)}(r,r,r)}$ , becomes the radial distribution function  $g(r)$ .

functions. Introducing  $\beta w^{(m)} = -\ln g^{(m)}$ ,  $g^{(3)} = g_{SA}^{(3)}G$  transforms into

$$w^{(3)}(\mathbf{r}_1, \mathbf{r}_2, \mathbf{r}_3) = w^{(2)}(\mathbf{r}_1) + w^{(2)}(\mathbf{r}_2) + w^{(2)}(\mathbf{r}_3) - \ln G/\beta \quad (1)$$

with  $w^{(2)}$  and  $w^{(3)}$  being the two- and three-particle potential of mean force, respectively. The equation shows that  $-\ln G \equiv \beta \Delta w^{(3)}$  plays the role of a three-body potential, measuring the (extra correlation) energy of three correlated particles relative to the energy of superposed correlated pairs of particles.

In an homogeneous, isotropic system,  $g^{(3)}$  depends on only three independent variables, chosen here to be  $r = |\mathbf{r}_1 - \mathbf{r}_2|$ ,  $s = |\mathbf{r}_2 - \mathbf{r}_3|$  and  $t = |\mathbf{r}_1 - \mathbf{r}_3|$ . Fig. (1) shows three-particle distribution functions in the equilateral triangle geometry for all three  $\Gamma$ 's considered. To allow comparison with the radial distribution function  $g(r)$  we have taken the cubic root  $\sqrt[3]{g^{(3)}(r,r,r)}$  so that  $\sqrt[3]{g_{SA}^{(3)}(r,r,r)} = g(r)$ . It is evident that the KSA, while working satisfactorily at low  $\Gamma$ , fails to reproduce the fine-structure of the triplet distribution function at higher

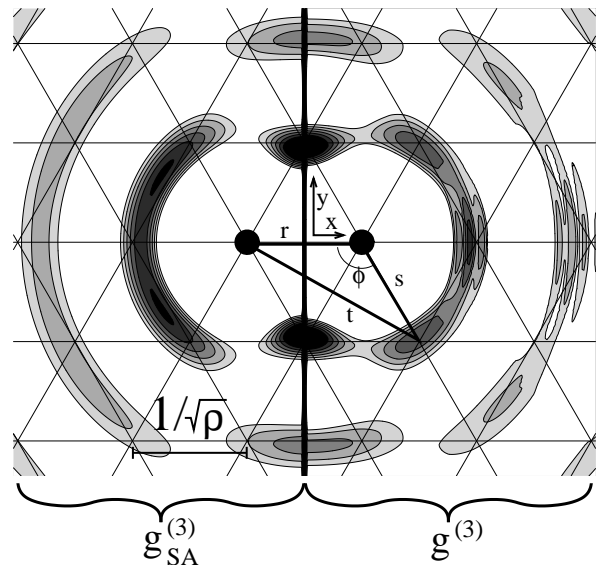


FIG. 2: Distribution functions  $g^{(3)}(r = r_{max}^{(2)}, s(x,y), t(x,y))$  (right half of the figure) and  $g_{SA}^{(3)}(r = r_{max}^{(2)}, s(x,y), t(x,y))$  (left half of the figure) in the  $(x,y)$ -plane ( $\Gamma = 46$ ). The missing half of each distribution is just the mirror-image of the one actually plotted. The constant  $g(r_{max}^{(2)})$  is subtracted from the distributions and only positive values are plotted with a grey-level scheme between white (zero) and black (max. value).

values of  $\Gamma$ . Obviously, correlations beyond the level of pair-correlations become important at higher  $\Gamma$ . To visualize  $g^{(3)}$  in two dimensions,  $r$  is fixed in the following to the distance  $r_{max}^{(2)}$  where  $g(r)$  has its first peak ( $\approx 1/\sqrt{\rho}$ ), so that  $g^{(3)}(r_{max}^{(2)}, s, t)$  varies just with  $s = s(x,y)$  and  $t = t(x,y)$  and can thus be plotted in the  $(x,y)$ -plane in form of a contour-plot. This is done in Fig. (2) for the  $\Gamma = 46$  measurement. We show in the left half of the figure  $g_{SA}^{(3)}$  and contrast it to the full three-particle distribution function  $g^{(3)}$ , plotted in the right half of the figure.  $g^{(3)}$  approaches  $g(r_{max}^{(2)})$  for large values of  $x^2 + y^2$ . To keep the figure as clear as possible, we plotted just those parts of  $g^{(3)} - g(r_{max}^{(2)})$  and  $g_{SA}^{(3)} - g(r_{max}^{(2)})$  that are larger than zero [26]. A hexagonal lattice with a lattice constant  $a = r_{max}^{(2)}$  is superposed. Both distributions  $g^{(3)}$  and  $g_{SA}^{(3)}$  reveal that the neighbors of the two central particles have positions which show a certain correspondence to the crystalline lattice points. However, while the banana-like structure of  $g_{SA}^{(3)}$  reflects just the coordination shells of the lattice, the full distribution function  $g^{(3)}$  shows a well-developed, angular dependent substructure, with individual peaks for almost every lattice point. This can be particularly well observed in the first coordination shell. Fig. (3) shows  $g^{(3)}$  and  $g_{SA}^{(3)}$  of Fig. (2) along the line  $(r = r_{max}^{(2)}, s = r_{max}^{(2)}, t = t(\phi))$ , which is a circle of radius  $r_{max}^{(2)}$  around the right particle in Fig. (2), passing through all lattice points of the particle's first

coordination shell (arrows in Fig. (3) mark positions of lattice points). It can be clearly seen that  $g^{(3)}$  develops peaks at the lattice points while  $g_{SA}^{(3)}$  completely fails to reflect the hexagonal structure. Also given is the function  $-\ln G$ , i.e.  $\Delta w^{(3)}$ , of eq. (1), now for all three values of  $\Gamma$  studied here. It is evident how  $\Delta w^{(3)}$  gradually forms on increasing  $\Gamma$ , with values up to one  $kT$  (in other regions of the  $(r, s, t)$ -space we find energies as high as  $2.5 kT$ !). It is also seen that the regions of attractive and repulsive correlation energies  $\Delta w^{(3)}$  correspond to the correcting effect which the function  $G$  has on  $g_{SA}^{(3)}$  to ensure that  $g^{(3)}$  adapts locally to the hexagonal symmetry. We conclude that it is an effect entirely due to three-particle correlations, i.e. due to the function  $G$ , which is responsible for the observed formation of a crystal-like local environment around particles well below the order-disorder transition. Clearly, in the ordered phase, one will ultimately observe peaks in  $g^{(3)}$  positioned exclusively on the lattice points. We also performed Monte-Carlo (MC) simulations using the above-given pair-potential  $\beta u(r) = \Gamma/(\sqrt{\pi}\rho r)^3$  (with a slightly better statistics than in the experiment: 250 configurations with 1000 particles). The almost perfect agreement between the distribution functions based on the MC-data (solid lines in Fig. (3)) and on the experimental configurations (symbols in Fig. (3)), demonstrate that there are virtually no contributions from many-body interactions, and that our model liquid consists of particles, interacting solely via pair-wise additive and precisely known potentials.

Triplet correlations play an important role in earlier liquid-state theories. Born and Green derived an equation [23, 27],

$$\frac{\partial w^{(2)}(r_{12})}{\partial \mathbf{r}_1} - \frac{\partial u(r_{12})}{\partial \mathbf{r}_1} = \rho \int \frac{\partial u(r_{13})}{\partial \mathbf{r}_1} \frac{g^{(3)}(\mathbf{r}_1, \mathbf{r}_2, \mathbf{r}_3)}{g(r_{12})} d\mathbf{r}_3, \quad (2)$$

relating the difference between the mean force and the direct pair-force to an integral over the force on particle 1 due to a particle at  $\mathbf{r}_3$ , weighted by the probability  $\rho g^{(3)} d\mathbf{r}_3 / g(r_{12})$  of finding a particle in  $d\mathbf{r}_3$  at  $\mathbf{r}_3$  when it is known that other particles are located at  $\mathbf{r}_1$  and  $\mathbf{r}_2$ . This equation is a member of the Born-Green-Yvon (BGY) hierarchy and is exact if pairwise interactions can be assumed. Inserting  $\beta w^{(2)} = -\ln g$  and using the KSA as a closure relation, eq. (2) yields the BGY integral equation for  $g(r)$ . Krumhansl and Wang used eq. (2) to check the accuracy of the KSA in their early simulations of a LJ fluid [10, 11]. Following their idea, we use experimental data to illustrate the importance of three-particle correlations. We numerically computed the right-hand side of eq. (2) using both the full and the approximated triplet function,  $g^{(3)}$  and  $g_{SA}^{(3)}$ , of the  $\Gamma = 4$  and  $\Gamma = 46$  measurement and compared it in Fig. (4) to the left-hand side of eq. (2), evaluated using  $u(r)$  and  $g(r)$ . For the weakly interacting system ( $\Gamma = 4$ ),  $G$  is unity in value everywhere (cf. Fig. (1 and (3))): triplet correlations are

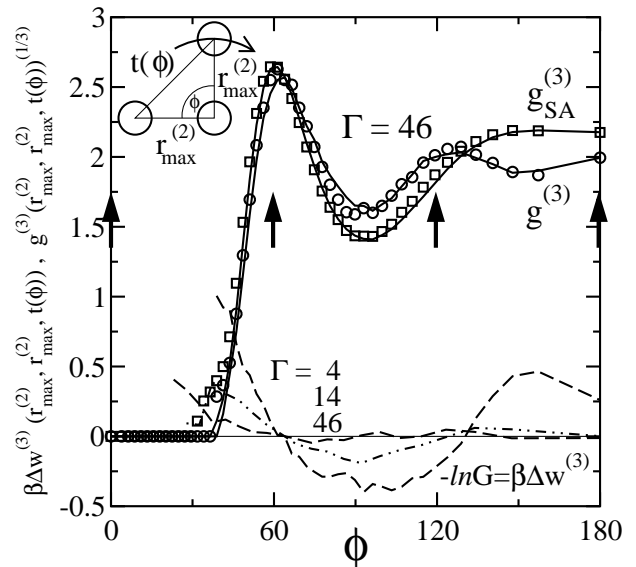


FIG. 3:  $g^{(3)}$  and  $g_{SA}^{(3)}$  from Fig. (2) for fixed values of  $r = r_{max}^{(2)}$  and  $s = r_{max}^{(2)}$ , as a function of the angle  $\phi$  (see inset). Symbols (solid lines) for distributions generated from measured (MC-simulated) configurations. Also given is the logarithm of the triplet correlation function  $G$ , which is related to the triplet correlation energy  $\Delta w^{(3)}$ , for  $\Gamma = 4$  (dashed line),  $\Gamma = 14$  (dashed-dotted line) and  $\Gamma = 46$  (dashed line).

unimportant, and, accordingly, the Born-Green equation can be satisfied with triplet functions based on the KSA, see Fig. (4). In the strongly interacting system ( $\Gamma = 46$ ), however, the KSA fails completely. Three-particle correlations have to be taken fully into account to obtain the correct difference between mean and direct force via the Born-Green equation. A number of other approximations for  $g^{(3)}$  are known [27], and can be checked in a similar way. This includes the Schofield equation [1], relating  $\partial g(r)/\partial \rho$  to  $g^{(3)}$ , which in turn is the basic equation for a number of thermodynamic consistency relationships [27]. From our results, we can expect that, here again,  $g^{(3)}$  at high  $\Gamma$  cannot be approximated, but has to be taken in its full form. Our results confirm predictions from simulation studies on LJ and hard-sphere systems showing that qualitatively the structure of  $g^{(3)}$  is correctly described by the KSA, but that quantitative failures can be appreciable [9, 13, 16, 28].

In summary, we used digital video microscopy and image processing on a PC to record the positional data of particles in a two-dimensional colloidal model liquid. From the measured configurations, we subsequently calculated particle correlation functions. The triplet correlation function contains much more information on the relative spatial arrangement of particles than the pair-correlation function. When the liquid is near the disorder-order transition, we have found that the deviations of the three-particle correlation function from unity are considerable (correlation energies as large as a few

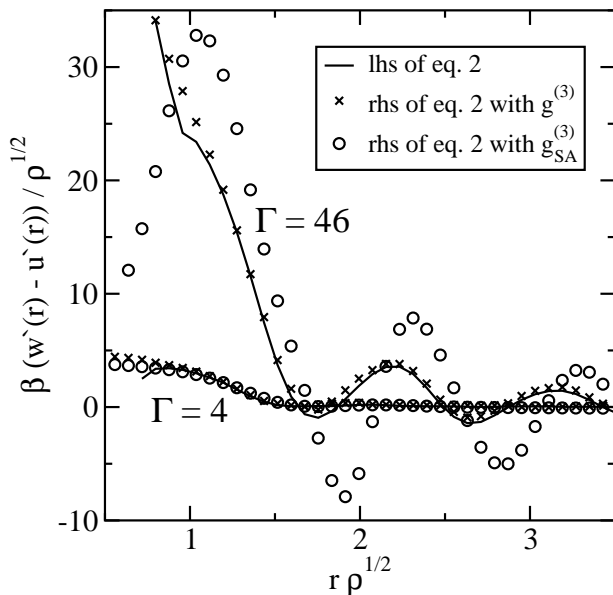


FIG. 4: Test of Kirkwood's approximation using experimentally determined three-particle distribution functions ( $\Gamma = 46$  and  $\Gamma = 4$ ). Solid lines for the left hand side of the Born-Green equation (eq. 2), symbols for the right hand side, evaluated using the full triplet distribution function  $g^{(3)}$  (crosses) and the distribution function  $g_{SA}^{(3)}$  (open circles) which is based on Kirkwood's superposition approximation.

$kT$ ), while states away from the disorder-order transition show smaller deviations. Furthermore, we have demonstrated that a quantitative understanding of triplet correlations is necessary to satisfy, for instance, the Born-Green equation. We close by remarking that from the measured configurations, higher-order correlation functions could be calculated as well, and that it soon will be possible to analyze higher-order correlation functions also in 3D colloidal samples, in much the same fashion as presented here, but with positional data recorded using modern confocal microscope techniques.

[1] P. Schofield, Proc. Phys. Soc. **88**, 149 (1966).

[2] G. Stell, J.C. Rasaiah, and H. Narang, Mol. Phys. **27**, 1393 (1974); W.G. Madden, D.D. Fitts, and W.R. Smith, Mol. Phys. **35**, 1017 (1978); C.G. Gray, K.E. Gubbins, and C.H. Twu, J. Chem. Phys. **69**, 182 (1978).

- [3] K. Scherwinski, Mol. Phys. **70**, 797 (1990).  
 [4] T. Lazaridis, J. Phys. Chem. B **104**, 16 (2000).  
 [5] H. Wang, M.P. Lettinga, and J.K.G. Dhont, J. Phys.: Condens. Matter **14**, 7599 (2002); J.K.G. Dhont and G. Nägele, Phys. Rev. E **58**, 7710 (1998).  
 [6] B.J. Alder, Phys. Rev. Lett. **12**, 317 (1964); E.A. Muller and K.E. Gubbins, Mol. Phys. **80**, 11 (1993).  
 [7] A. Rahman, Phys. Rev. Lett. **12**, 575 (1964).  
 [8] S. Gupta, J.M. Haile, and W.A. Steele, Chem. Phys. **72**, 425 (1982).  
 [9] J.A. Krumhansl and S.S. Wang, J. Chem. Phys. **56**, 2034 (1972).  
 [10] J.A. Krumhansl and S.S. Wang, J. Chem. Phys. **56**, 2179 (1972).  
 [11] S.S. Wang and J.A. Krumhansl, J. Chem. Phys. **56**, 4287 (1972).  
 [12] H.J. Raveche and R.D. Mountain, in *Progress in liquid physics*, edited by C.A. Croxton (Wiley, New York, 1978).  
 [13] W.J. McNeil, W.G. Madden, A.D.J. Haymet, and S.A. Rice, J. Chem. Phys. **78**, 388 (1983).  
 [14] P. Linse, J. Chem. Phys. **94**, 8227 (1991); Y. Tanaka and Y. Fukui, Prog. Theor. Phys. **53**, 1547 (1975); S. Jorge, E. Lomba, and J.L.F. Abascal, J. Chem. Phys. **117**, 3763 (2002).  
 [15] G. Hummer and D.M. Soumpasis, J. Chem. Phys. **93**, 581 (1993).  
 [16] F. de J. Guevara-Rodriguez and M. Medina-Noyola, Mol. Phys. **95**, 621 (1998).  
 [17] J.G. Kirkwood, J. Chem. Phys. **3**, 300 (1935).  
 [18] S.A. Rice and J. Lekner, J. Chem. Phys. **42**, 3559 (1965).  
 [19] R.N. Sane, Phys. Rev. A **25**, 1779 (1982).  
 [20] P. Attard, J. Chem. Phys. **95**, 10 (1991).  
 [21] M. Fushiki, Mol. Phys. **74**, 307 (1991).  
 [22] D.J. Winfried and P.A. Egelstaff, Can. J. Phys. **51**, 1965 (1973); P.A. Egelstaff, D.I. Page, and C.R.T. Heard, Phys. Lett. A **30**, 376 (1969); W. Montfrooij, L.A. de Graaf, P.J. van der Bosch, A.K. Soper, and W.S. Howells, J. Phys.: Condens. Matter **3**, 4089 (1991); P.A. Egelstaff, Ann. Rev. Phys. Chem. **24**, 159 (1973).  
 [23] M. Born and H.S. Green, Proc. R. London Soc. Ser. A **188**, 10 (1946); J. Yvon, Actualities Scientifiques et Industriel **203**, 1 (1935).  
 [24] K. Zahn, R. Lenke, and G. Maret, Phys. Rev. Lett. **82**, 2721 (1999).  
 [25] K. Zahn and G. Maret, Phys. Rev. Lett. **85**, 3656 (2000).  
 [26] The stripes that can be seen especially close to the x-axis result from the transformation  $g^{(3)}(r_{max}, s, t)$  to  $g^{(3)}(r_{max}, x, y)$  and appear due to limited statistics.  
 [27] P.A. Egelstaff, *An Introduction to the Liquid State* (Oxford University Press, Oxford, 1992).  
 [28] H.J. Raveche, R.D. Mountain, and W. B. Streett, J. Chem. Phys. **61**, 1970 (1974).